



Contents lists available at ScienceDirect

J. Vis. Commun. Image R.

journal homepage: www.elsevier.com/locate/jvci



Short Communication

A method for sparse disparity densification using voting mask propagation

J. Ralli *, J. Díaz, E. Ros

Departamento de Arquitectura y Tecnología de Computadores, Escuela Técnica Superior de Ingenierías y de Telecomunicación, Universidad de Granada, Calle Periodista Daniel, Saucedo Aranda s/n, E-18071 Granada, Spain

ARTICLE INFO

Article history:
Received 31 October 2008
Accepted 20 August 2009
Available online xxx

Keywords:
Disparity densification
Voting propagation

ABSTRACT

We describe a novel method for propagating disparity values using directional masks and a voting scheme. The driving force of the propagation direction is image gradient, making the process anisotropic, whilst ambiguities between propagated values are resolved using a voting scheme. This kind of anisotropic densification process achieves significant density enhancement at a very low error cost: in some cases erroneous disparities are voted out, resulting not only in a denser but also a more accurate final disparity map. Due to the simplicity of the method it is suitable for embedded implementation and can also be included as part of a system-on-chip (SOC). Therefore, it can be of great interest to the sector of the machine vision community that deals with embedded and/or real-time applications.

© 2009 Elsevier Inc. All rights reserved.

1. Introduction

Disparity is originally defined as being the horizontal difference of a 3D point being projected on two adjacent imaging devices (e.g. stereo-rig) and if both intrinsic- and extrinsic parameters of the imaging system are known, complete 3D-reconstruction of the scene is possible. However, even if we do not know all the necessary parameters to do a complete 3D-reconstruction, disparity still conveys relative information of the 3D structures of the scene which can also be useful.

Disparity extraction models are based on local or global optimization methods that minimize (or maximize) matching cost of image features between two or more images. Practically all the sparse models have some kind of threshold or other parameter, either implicit or explicit, which affects density and at the same time error in the derived disparity map [1,2]. On the other hand, the global methods that minimize energy functions within the whole scene, through local operations, usually derive a disparity map that is typically 100% dense (sometimes detecting occlusions as well). Such global minimization can be done using different approaches such as variational methods [3–7] or graph cuts [8,9]. Typically, depending upon the sparse method used, as density increases, after a certain limit error also starts to increase concomitantly. Therefore, it is worth calculating a less dense, high-confidence disparity map and afterwards increasing the density by propagating the correct disparity values. In this

way we achieve better accuracy vs. density trade-off than by directly reducing the reliability threshold and thus increasing density at the expense of higher error. Many global, dense, disparity calculation methods have built-in mechanisms for propagating/diffusing disparity [4,10] but sparse methods usually lack this capacity. To the best of our knowledge there are very few independent propagation methods, apart from interpolation [11] and diffusion [12], that can be applied as a post-processing step. By independent we mean that the propagation method does not depend upon the algorithm used to derive the initial disparity map. This work proposes a new densification method that is able to arrive at denser and more accurate results than the standard one-stage disparity algorithms such as dynamic programming, block-matching and so on that only slightly affects the error rate. Since the scheme is based on very simple operations, it can be considered suitable for efficient implementation. Our method resembles image driven anisotropic diffusion, used for instance by Alvarez et al. [4] in variational disparity calculation, in the sense that the propagation direction is based on the image gradient. Instead of using a set of equations for defining the diffusion model as it is done in [4] our approach (VMP) uses a bank of predefined masks and a voting process to define the local interactions driving the diffusion process.

2. Method

The first step is to calculate a sparse, high-confidence, stereo map. Many feature-based disparity calculation methods match edges present in stereo-images, since these can be considered rel-

* Corresponding author. Fax: +34 958 248993.
E-mail addresses: jarno@ralli.fi, jarnor@atc.ugr.es (J. Ralli), jdiaz@atc.ugr.es (J. Díaz), eros@atc.ugr.es (E. Ros).

actively robust features [13,14]. For the reasons set out in Section 1 we use here a simplified dynamic programming technique based on image edges [11]. The rationale for using dynamic programming is that it has been shown to be both computationally efficient [15] and capable of producing highly accurate results [2]. Nevertheless, as mentioned earlier, our densification approach does not depend upon the method used for producing the initial sparse disparity map. The second step is to apply voting mask propagation (VMP) for propagating disparity in the direction where estimations are expected to be similar and to use voting for resolving ambiguities. Local support of the voting process is based on directional masks: for each image position for which disparity is known a mask from a pre-determined bank is chosen, depending upon the underlying image structure (gradient). The properties of the chosen filter define how many votes each of the neighborhood positions will receive.

2.1. Propagation direction

Since without further image analysis we cannot be sure of which object an image pixel for which the disparity is known belongs to, and since we assume that inside objects disparity changes gradually, image gradient is used as a driving force of the propagation direction. We assume that two different objects will almost certainly have two different disparity levels. By propagating in a direction perpendicular to the image gradient we reduce errors since different objects have varying disparities divided by an edge. This assumption of local maximum gradient separating different objects is also the basis of anisotropic diffusion, where diffusion direction is driven by the gradient [12,16]. In this work we concentrate on the case where the disparities for the edges are known and the disparities are propagated in an edge-wise direction. There is, however, no reason why the disparities not residing at the edges could not be propagated as well. The tangent-to-edge direction is approximated by calculating image gradient.

2.2. Bank of masks

A bank of masks is designed using a 2D multivariate Gaussian distribution which is rotated in order to generate masks corresponding to different propagation directions. The basic mask, corresponding to orientation 0° (i.e. the horizontal axis), is calculated as per the following equation:

$$z = G(i, j, \mu_i = \mu_j = 0, \Sigma), \quad i = -N \dots N, \quad j = -P \dots P \quad (1)$$

where $G()$ denotes multivariate Gaussian, (i, j) are the coordinates of the mask, $(\mu_i = \mu_j = 0)$ are the mean, Σ is the covariance, z is the number of votes that each position receives and N and P define the mask size. Fig. 1 shows a voting mask corresponding to several different orientations (rotations).

The use of Gaussian distribution is motivated by the fact that it reflects the probabilistic nature of our approach: the underlying image structure drives the propagation direction and thus reflects our belief on how the disparity is distributed. Other authors have used similar approaches for image denoising [17]. Furthermore, Gaussian multivariate distribution allows a smooth transition from isotropic to anisotropic cases, depending on the certainty of the image structure, which can be used in more elaborated schemes by further analyzing the image. Besides a Gaussian distribution can be implemented as a separable convolution thus making it efficient computationally.

2.3. Choosing the mask

Once the orientations of the edge tangents have been approximated, propagation is carried out for each disparity value using the mask whose orientation best matches the tangent of the edge. The most closely corresponding masks centre is placed on top of the disparity value of interest and each pixel within mask size receives as many votes for the disparity value as defined by the mask. This is shown in the following equation:

$$V_{x+i, y+j}(D_{x,y}) = G_{x,y,\Delta}(x+i, y+j), \quad i = -N \dots N, \quad j = -P \dots P \quad (2)$$

where $V_{x,y}$ indicates votes received by position (x, y) for disparity, D , $G_{x,y,\Delta}(x+i, y+j)$ denotes how the Gaussian voting mask, chosen as per gradient Δ , with a size of $(2N+1, 2P+1)$, placed at (x, y) votes for each mask position. As a final step, after the disparities have been propagated for each of the original disparity values, each pixel position assumes the disparity that receives most votes, as defined in the following equation:

$$D_{x,y} = \max_v(V_{x,y}, D_{x,y}) \quad (3)$$

where $D_{x,y}$ indicates the final chosen disparity value for a position (x, y) and $\max_v(V, D)$ returns the disparity value that has received the most votes for a set of vote-disparity tuples (V, D) . Due to the spatial support of the voting mechanism erroneous values are in certain cases effectively voted out: if within a certain neighborhood there are more correct values than erroneous val-

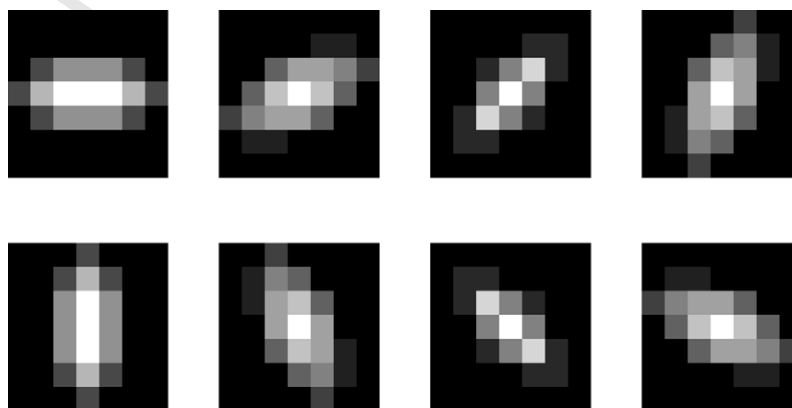


Fig. 1. A bank of 7×7 voting masks corresponding to different orientations. Intensity codifies the number of votes each position receives.



Fig. 2. Results for the test images: the left-hand column contains left-hand images of the original stereo-pairs, the middle column shows disparity maps calculated by dynamic programming and the right-hand column disparity maps densified using VMP. C denotes the percentage of correct disparities (± 1 disparity level) and D, density.

165 ues, the erroneous values receive fewer votes and are discarded.
 166 Interestingly enough this effect allows the densification process
 167 to arrive at a denser but at the same time more accurate
 168 map than the original.

2.4. Pseudocode

169
 170 For the sake of clarity, below we have included a pseudocode of
 171 the propagation process.


```

173 //I input image driving the voting process
174 //D disparity map
175 //M bank of masks (mask size (N,P))
176 //V a matrix for storing the votes (initialize to 0)
177
178 //- VOTE- -
179 //Obtain coordinates for disparities
180 (x y) = coords(notEmpty(D))
181 for j = 1: numel(x)
182 //Choose the closest mask corresponding to gradient normal
183  $\Delta I = \text{calculateImageGradient}(I(x(i),y(i)))$ 
184 mask = chooseMask(M,  $\Delta I$ )
185 //Vote using the chosen mask
186  $V = \text{vote}(x(i), y(i), \text{mask}, D(x(i),y(i)), N, P)$ 
187 end
188 //- CHOOSE WINNERS- -
189 (x y) = coords(notEmpty(V))
190 for j = 1: numel(x)
191  $\text{Out}(x(i),y(i)) = \text{MAX}(V(x(i),y(i)))$ 
192 end
    
```

193
194 The actual voting process can be seen as superimposition of the
195 chosen mask on top of the disparity value to be propagated where
196 each neighboring pixel (defined by the mask) receives as many

197 votes for the disparity as defined by the weight of the mask as each
198 position. For each pixel position the number of votes for each dis-
199 parity needs to be stored so that a winner can be chosen
200 accordingly.

201 **3. Experiments and results**

202 We benchmarked the method using well known stereo-images
203 available at <http://www.vision.middlebury.edu/stereo/>. In order to
204 study how the VMP densification process behaves when dealing
205 with different initial densities and/or errors, we have used two
206 different methods for generating the initial disparity maps provided
207 to the VMP model. The different methods used were dynamic pro-
208 gramming (DP) [11] and a phase-based method [1,18]. Further-
209 more, we have used different thresholds and interleave factors
210 for DP in order to generate initial disparity maps with different
211 densities and errors. Computational complexity of the our method
212 was approximated by comparing it with execution times of the DP
213 method. We also introduce a sample application that clearly bene-
214 fits from a more dense disparity map as input. In the experiments,
215 size of the propagation masks was 7×7 pixels. Density is given in
216 terms of a ratio between the number of pixels for which disparity
217 has been defined and the total number of pixels in the image. Over-
218 all accuracy is measured as the percentage of correct pixels (± 1
219 disparity level) calculated against the ground-truth values.

220 **3.1. Results**

221 Fig. 2 shows the original stereo-pair images and results calcu-
222 lated directly using DP and densified by VMP.

223 Fig. 3 demonstrates the results for four different initial maps
224 with different densities. The initial maps are calculated using dif-
225 ferent thresholds for occlusion detection with the effect of increas-
226 ing density at the expense of accuracy. Thus it can be observed that
227 after certain reasonable limit, in order to obtain even more dense
228 map, the error starts to increase. In such a case it is better to calcu-
229 late more reliable initial map and then densify.

230 Fig. 4 shows the results for the Venus case only. It can be clearly
231 seen that as the cost for occlusions gets higher (threshold from one
232 to four) density of the resulting disparity map increases slightly at
233 the expense of accuracy. On the other hand, as the error increases

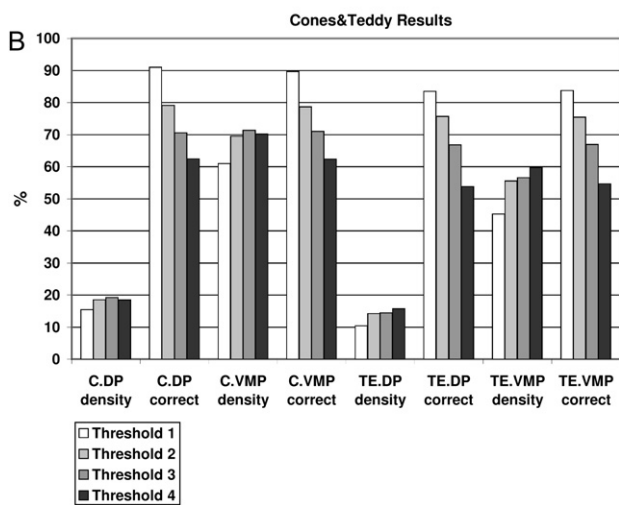
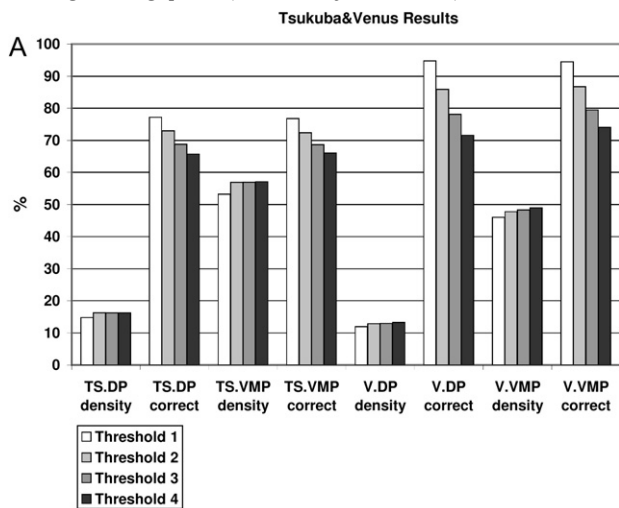


Fig. 3. Densification results for several initial densities obtained using different thresholds for dynamic programming. DP refers to results calculated by directly using dynamic programming and VMP refers to results densified from corresponding DP results using voting mask propagation. (A) TS refers to Tsukuba and V refers to Venus images and (B) C refers to Cones and TE refers to Teddy images.

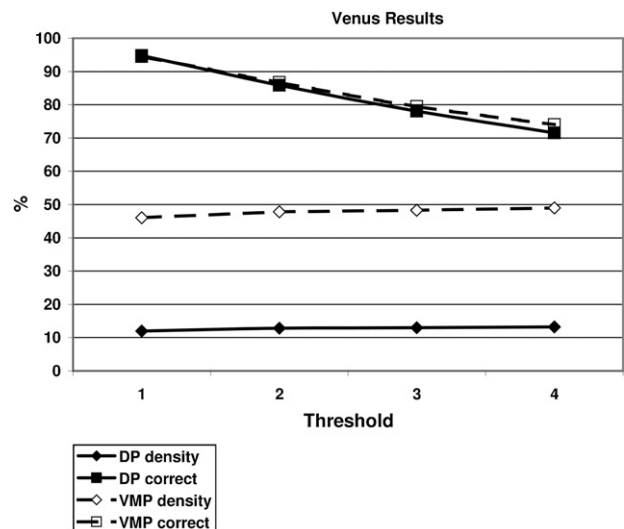


Fig. 4. Densification results for several initial densities obtained using different thresholds in dynamic programming. DP refers to dynamic programming and VMP to voting mask propagation. Density refers to the density of the obtained disparity map and correct refers to the percentage of correct disparities (± 1 disparity level).

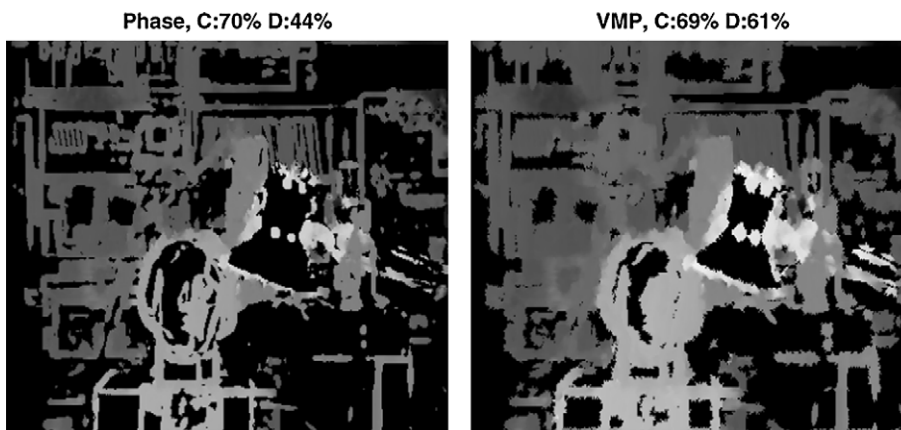


Fig. 5. Phase refers to phase-based method and VMP to voting mask propagation. C denotes the percentage of correct disparities (± 1 disparity level) and D, density.

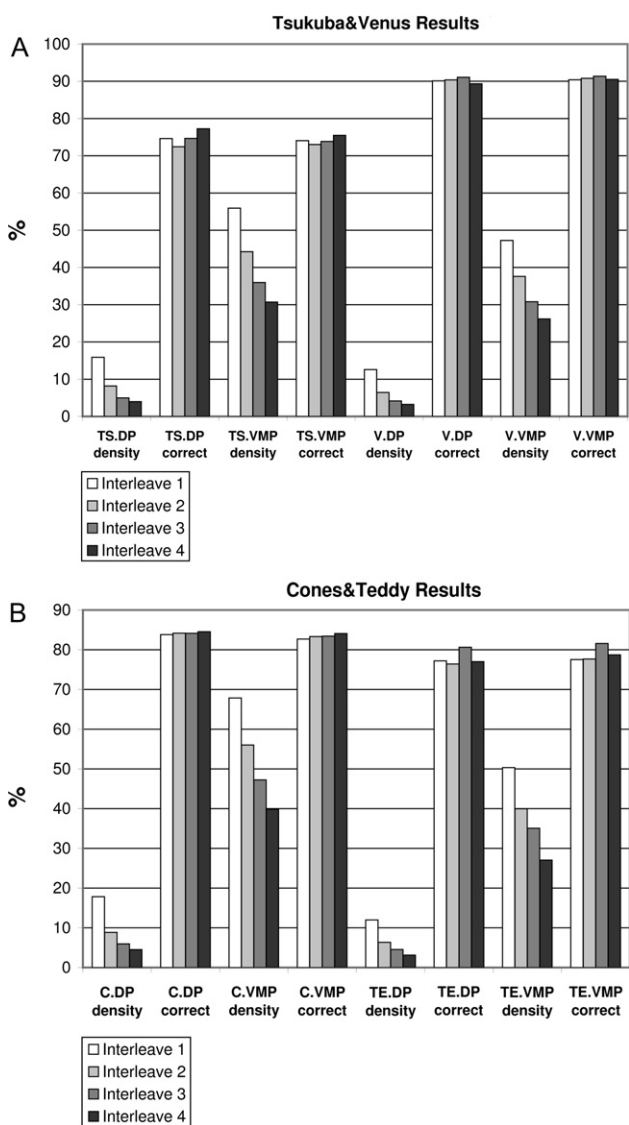


Fig. 6. Densification results for several initial densities obtained using different interleaves for dynamic programming. DP refers to results calculated by directly using dynamic programming and VMP refers to results densified from corresponding DP results using voting mask propagation. (a) TS refers to Tsukuba and V refers to Venus images and (b) C refers to Cones and TE refers to Teddy images.

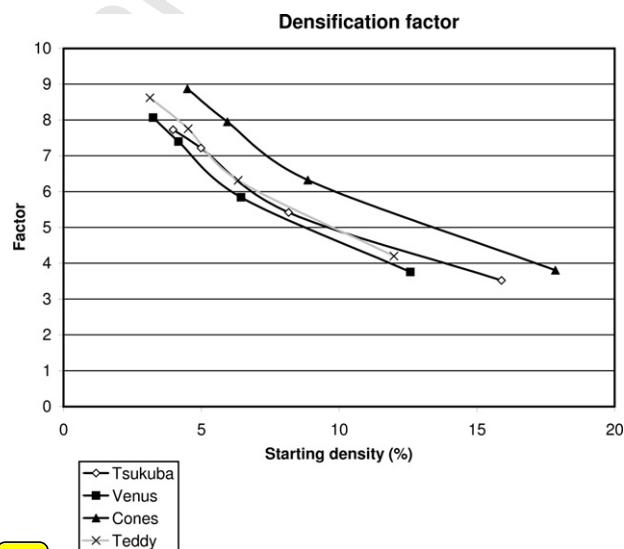


Fig. 7. Densification factor results for different initial disparities. Y-axis shows the density of the initial map while X-axis displays the obtained densification factor.

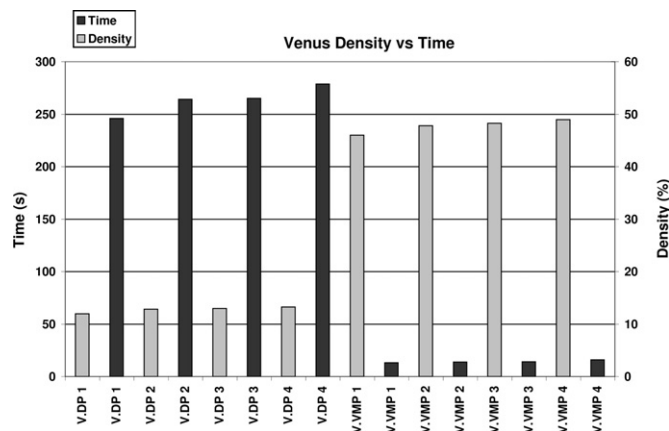


Fig. 8. Computation times for both the dynamic programming and the voting mask propagation methods. DP refers to dynamic programming and VMP to voting mask propagation.

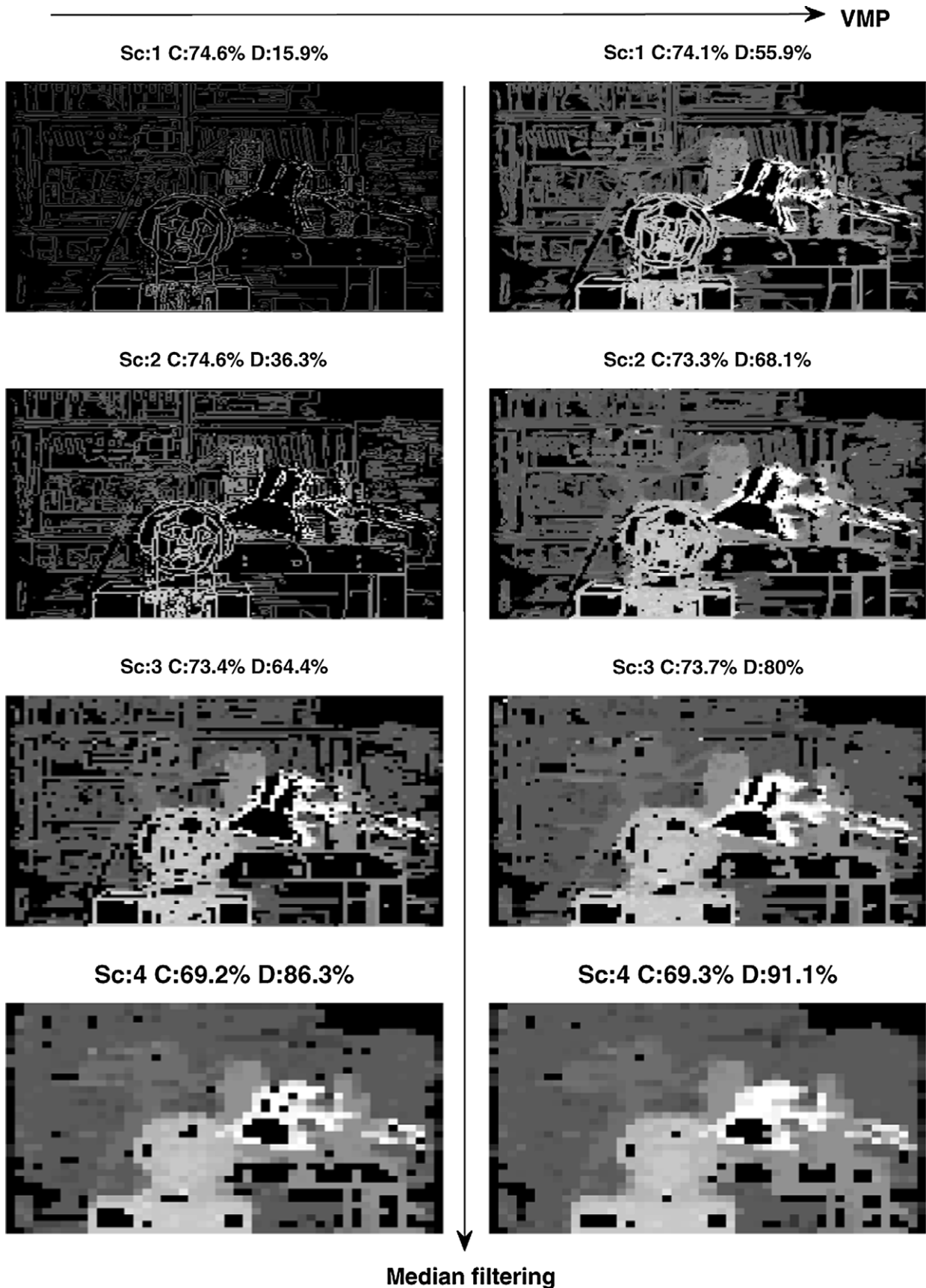


Fig. 9. Down-scaling results using a median filter: the left-hand column contains results of down-scaling Tsukuba disparity calculated using dynamic programming, whilst that on the right shows the results of applying VMP on the first scale and then down-scaling. Sc denotes the scale, while C and D denote percentage of correct disparities (± 1 disparity level) and density.

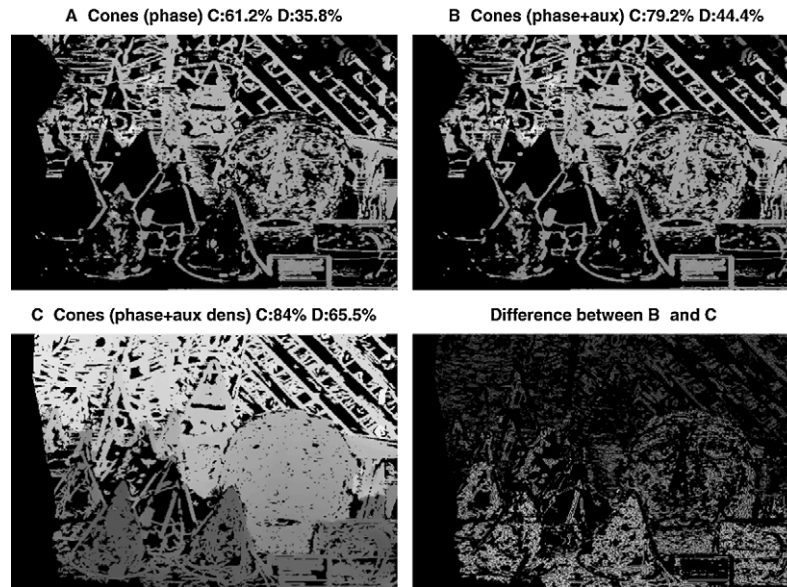


Fig. 10. Dense-disparity calculation results: (A) without fusion; (B) fusion using sparse-disparity with 15% density (C) fusion using sparse-disparity with 60% density and (D) the difference between (B) and (C). C denotes the percentage of correct disparities and D, density.

the voting mechanism starts to vote out some of the erroneous values thus increasing the accuracy.

Fig. 5 displays densification results using an initial disparity map calculated by a phase-based method [18]. Density and error of the resulting densified map is similar to the rest of the results even though the starting density with this technique is significantly higher than in the previous experiments based on dynamic programming.

Figs. 6 and 7 demonstrate the results of different initial disparities upon the densified disparity and the obtained densification factor. Different initial density disparities were obtained using DP with different vertical line interleaves (interleave 1 = disparity calculated for all the vertical lines; interleave 2 = disparity calculated for every second line, etc.). This experiment demonstrates both robustness of the VMP method in relation to initial density and what kind of densification factors can be expected. As the density of the input map increases the densification factor decreases which is due to overlapping of the propagation filters.

Fig. 8 displays the computational times of both the dynamic programming and the voting mask propagation methods, implemented in Matlab. The four different cases correspond to the four different thresholds already seen in Fig. 3. This kind of a comparison is approximate since it depends on implementation issues but, however, it does give a valuable hint of the relative computational complexities.

In applications where less resolution is needed, further densification can be achieved by down-scaling. Fig. 9 shows the results of down-scaling disparity maps by a factor of two, using a 2×2 median filter and discarding those pixels that do not have a disparity estimation. In order to calculate the percentage of correct disparities, each of the downscaled disparity maps was upscaled to the same size as the ground-truth.

3.2. Sample application

We present here a specific application which benefits from a denser sparse-disparity map: fusion of sparse- and dense-disparity stereo [19] for disambiguation of dense disparity estimations. In the framework of DRIVSCO [19] Ralli et al. have demonstrated the benefits of using symbolic, reliable sparse-disparity to disambiguate unclear cases in dense-disparity calculation. We tested

the fusion scheme, with different sparse-disparity densities, upon a hardware simulation of a phase-based [1,18] disparity calculation method with and without fusion. The hardware simulation approximates a realtime FPGA implementation (currently being implemented at the University of Granada) of the phase-based method. Due to limited on-chip computational resources the implementation requires a trade-off between accuracy and efficiency. In such a scheme where external approximations are available, these can be used to guide the dense method and thus the accuracy can be restored as shown in Fig. 10. As can be seen in Fig. 10, the fusion process benefits clearly from a denser sparse-disparity map used to guide the dense disparity calculation method.

4. Conclusion

We have shown that our novel method of propagating sparse disparity information based on directional masks and a voting scheme is capable of significantly increasing density with a very minor increase in overall error, thus considerably enhancing the initial sparse disparity map. Further densification can be achieved by down-scaling, by active interpolation [20–22] or by diffusion [12]. Even though in this study we have used VMP for propagating binocular visual information based on monocular cues, VMP can also be used for propagating other visual cues, such as optical flow and others. The simplicity of the method facilitates its efficient implementation.

Acknowledgments

This work was supported by the EU research Project DRIVSCO (IST-016276-2) and the Spanish Grants DINAM-VISION (DPI2007-61683), RECVIS (TIN2008-06893-C03-02), P06-TIC-02007 and TIC-3873. The authors thank A.L. Tate for revising their English text.

References

- [1] F. Solari, S. Sabatini, G. Bisio, Fast technique for phase-based disparity estimation with no explicit calculation of phase, *Electronics Letters* 37 (23) (2001) 1382–1383.

- 308 [2] M. Brown, D. Burschka, G. Hager, Advances in computational stereo, *Pattern*
309 *Analysis and Machine Intelligence* 25 (8) (2003) 993–1008. 336
- 310 [3] B. Horn, B. Schunck, Determining optical flow, *Artificial Intelligence* 17 (1981)
311 185–203. 337
- 312 [4] L. Alvarez, R. Deriche, J. Sánchez, J. Weickert, Dense disparity map estimation
313 respecting image discontinuities: a PDE and scale-space based approach,
314 *Journal of Visual Communication and Image Representation* 13 (1) (2002) 3–
315 21. 338
- 316 [5] J.W. Lee, J. Sánchez, Reliable estimation of dense optical flow fields with
317 large displacements, *International Journal of Computer Vision* 39 (1) (2004)
318 41–56. 339
- 319 [6] T. Brox, From pixels to regions: partial differential equations in image analysis,
320 Ph.D. Thesis, Saarland University, 2005. 340
- 321 [7] O. Faugeras, R. Keriven, Level set methods and the stereo problem, in:
322 *Proceedings of the First International Conference on Scale-Space Theory in*
323 *Computer Vision*, 1997, pp. 272–283. 341
- 324 [8] V. Kolmogorov, Graph based algorithms for scene reconstruction from two or
325 more views, Ph.D. Thesis, Cornell University, 2003. 342
- 326 [9] V. Kolmogorov, R. Zabini, What energy functions can be minimized via graph
327 cuts?, *Pattern Analysis and Machine Intelligence* 26 (2004) 147–159 343
- 328 [10] D. Scharstein, R. Szeliski, Stereo matching with non-linear diffusion,
329 *International Journal of Computer Vision* 28 (2) (1998) 155–174. 344
- 330 [11] J. Ralli, F. Pelayo, J. Díaz, Increasing efficiency in disparity calculation, in:
331 *BVAI2007*, vol. 4729, 2007, pp. 298–307. 345
- 332 [12] J. Weickert, Anisotropic diffusion in image processing, Ph.D. Thesis, Universität
333 Kaiserslautern, 1998. 346
- 334 [13] X. Jiangjian, S. Mubrak, Two-frame wide baseline matching, in: *Proceedings of*
335 *the ICCV'03*, 2003, 2003, pp. 603–609. 347
- [14] N. Krüger, M. Felsberg, An explicit and compact coding of geometric and
336 structural information applied to stereo matching, *Pattern Recognition Letters*
337 25 (8) (2004) 849–863. 338
- [15] G. Minglun, Y. Yee-hong, Real-time stereo matching using orthogonal
339 reliability-based dynamic programming, *IEEE Transactions on Image*
340 *Processing* 16 (3) (2007) 879–884. 341
- [16] P. Perona, J. Malik, Scale-space and edge detection using anisotropic diffusion,
342 *IEEE Transactions on Pattern Analysis and Machine Intelligence* 12 (1990)
343 629–639. 344
- [17] D. Cho, T.D. Bui, Multivariate statistical modeling for image denoising using
345 wavelet transforms, *Signal Processing: Image Communication* 20 (1) (2005)
346 77–89. 347
- [18] S. Sabatini, G. Gastaldi, F. Solari, J. Diaz, E. Ros, K. Pauwels, M.V. Hulle, N.
348 Pugeault, N. Krüger, Compact and accurate early vision processing in the
349 harmonic space, in: *Proceedings of VISAPP*, vol. 1, 2007, pp. 213–220. 350
- [19] J. Ralli, Disparity disambiguation by fusion of signal- and symbolic-level
351 information, Tech. Rep., University of Granada, DRIVSCO EU-Project (FP6-IST-
352 FET, Contract 016276-2), Learning to Emulate Perception-Action Cycles in a
353 Driving School Scenario, 2008. Project web-page available at [http://](http://www.pspc.dibe.unige.it/drivSCO/)
354 www.pspc.dibe.unige.it/drivSCO/. 355
- [20] H. Yoo, Closed-form least-squares technique for adaptive linear image
356 interpolation, *Electronics Letters* 43 (4) (2007) 210–212. 357
- [21] L. Zhang, W. Xiaolin, An edge-guided image interpolation algorithm via
358 directional filtering and data fusion, *IEEE Transactions on Image Processing* 15
359 (2006) 2226–2238. 360
- [22] H.C. Ting, H.M. Hang, Edge preserving interpolation of digital image using
361 fuzzy inference, *Journal of Visual Communication and Image Representation* 8
362 (4) (1997) 338–355. 363
- 364